

Swaged bolts: modelling of the installation process and numerical analysis of the mechanical behaviour

M. Dréan^a, A.-M. Habraken^b, A. Bouchaïr^a, J.-P. Muzeau^{a,*}

^a LERMES/CUST, Blaise Pascal University, BP 206, 63174 Aubière Cedex, France

^b M&S, Bat B5213, Chemin des Chevreuils 1, University of Liège, B4000 Liège 1, Belgium

Abstract

Swaged bolts are an alternative to high strength bolts in steel structures. To clarify the steps of the installation process, numerical modelling has been carried out. The relevant phenomena are described and evaluated. This numerical calculation accounts for large displacements, large strains, mechanical plasticity and friction contact between the components of swaged bolts. The non-linear finite element code "Lagamine" designed for the simulation of metal forming processes has been used to provide the stress distributions in the components.

Keywords: Swaged bolts; HSFG bolts; Bolt modelling; Installation process; Numerical analysis; Metal forming; Friction contact

1. Introduction

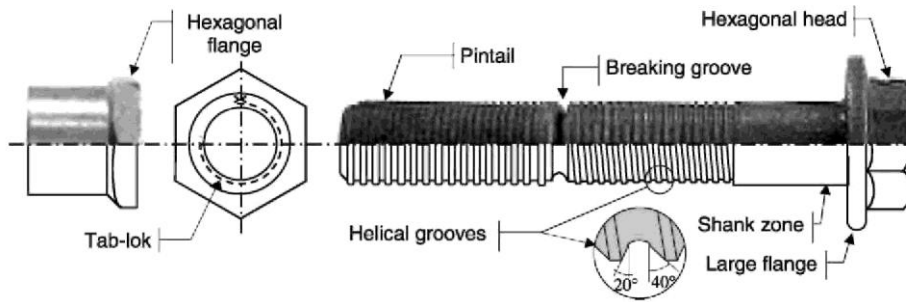
Swaged bolts are an alternative to high strength friction grip (HSFG) bolts for connections in steel structures. Because of their automatic installation process, the installed preload is expected to be established with reasonable confidence. In Europe, the mechanical knowledge about this fastener raised from tests carried out to qualify the bolts [1-3]. Nevertheless, some unexpected mechanical results (too low preload value, loss of the preload [2]) appeared during installation tests. Therefore, it was decided to use a numerical modelling to describe and to evaluate the influences of the different steps of the installation process on the preload. First, this paper contains a description of the bolt. Then, the finite element software Lagamine is presented. It allows practical applications with large strains, large rotations and/or large displacements and accounts for friction between elements. After a detailed description of the modelling of each bolt component (geometry and mechanical characteristics), the calculation results are given. Especially, the way the force is transferred from the hydraulic installation tool into the bolt is explained. Finally, the stress distribution is analysed and related to the low-cycle fatigue behaviour shown during tests.

2. General presentation of swaged bolts

2.1. Description of the basic components

Like classical HSFG bolts, prestressed swaged bolts are made up of two different components (Fig. 1). The pin acts as a bolt screw with a shank zone chosen according to the thickness of the plates. The collar acts as a nut whose threads are created during the installation process. The available pin diameters are 12, 16, 20, 24 and 27 mm. Their geometrical and mechanical characteristics are nearly the same as those of high strength bolts grade 10.9 or A490 [1]. The main geometrical characteristic of these bolts is the thread: a helical groove with a special profile showing a succession of linear and elliptical parts. The flat sides are orientated at 20° and at 40° instead of 30° as in a traditional thread.

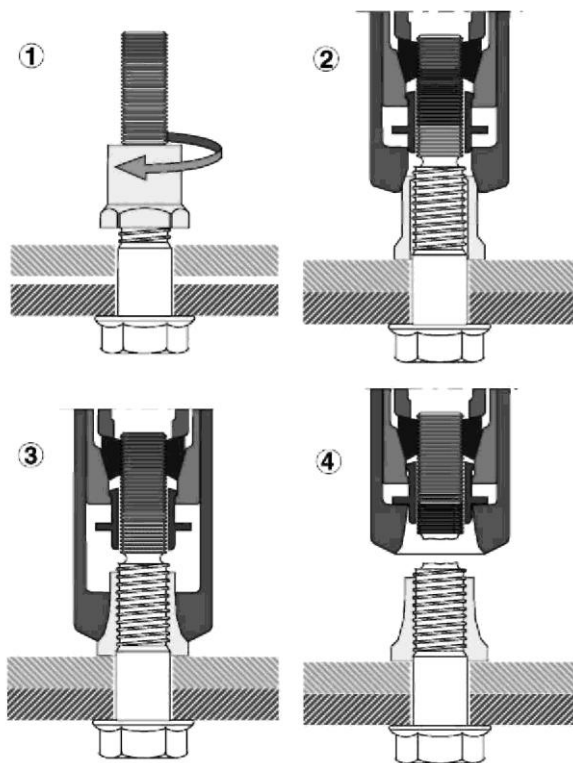
Fig. 1. Collar and pin of a swaged bolt.



2.2. Installation process and advantages of swaged bolts

The installation process of swaged bolts is completely different from a classical bolt strengthening and it represents the major advantage of this type of fastener. It consists of swaging the collar onto the pin with a special hydraulic tool. It is nearly the same installation as rivet installation. The internal diameter of the hydraulic tool nose (anvil), is smaller than the external diameter of the collar. Therefore, the collar material flows into the pin grooves. This process of installation creates a bond without any gap. So the self-unscrewing of this kind of bolts is nearly impossible. It argues for the use of these fasteners in applications under vibrations (truck body for instance). Moreover, the installation is very fast: less than 30 s per bolt. In civil engineering, where the number of bolts can be large (thousands), it is beneficial to minimise the installation time without any lack of accuracy on the preload.

Fig. 2. Installation process.



The sequence of the installation process can be divided into four steps (Fig. 2). First (1), the pin is inserted through a prepared hole and the collar is threaded onto the pin using a unique small prethread called "tab-lok". Then, the nose assembly of the hydraulic tool is placed over the pintail. The hydraulic pressure makes the tool

pull on the pintail and press the plates together (2). The anvil pushes on the collar. Continued pulling on the pintail moves the anvil forward, swaging the collar into the pin grooves. This swaging action lengthens the collar and develops a permanent clamp force (preload) in the pin. When swaging is completed (3), the contact between the different elements allows the pulling load to increase up to break the breaking groove. So, the pintail separates from the pin and the anvil disengages from the collar (4).

This automatic and fast installation process allows a preload to be installed when the connected plates respect the out-of-flatness tolerances. The value of this preload is in the same range of the preload value installed in a HSFG bolt of the same diameter. Nevertheless, some tests carried out to check the value of the installed preload [2,3] have shown that a large out-of-flatness defect can affect significantly the value of the preload. So a FEM simulation of the process has been used to provide a better understanding of the successive phenomena appearing during the installation process.

3. General presentation of the finite element code Lagamine

3.1. Introduction

Since 1984, the Lagamine software has been developed at the University of Liege by Cescotto's team to simulate metal forming processes. For instance, rolling [4], deep drawing [5], extrusion and forging [6] processes have been studied and couplings with microscopic events like recrystallization [7] or texture evolution [8] have been investigated. Two-dimensional or three-dimensional analyses, mechanical or thermo-mechanical simulations are available. This code provides both solid and contact finite elements as well as a large library of constitutive laws.

Working in a frame of solid mechanics with large strains, large rotations and/or large displacements, the code is characterised by different choices:

- Lagrangian formulation meaning that the mesh sticks to the solid,
- hypo-elastic formulation where elastic and plastic strain rates are directly added and no constitutive equation is required for plastic spin. This choice remains physically sound as long as elastic strains are small,
- use of Cauchy stresses and Jaumann derivatives to express objective constitutive laws,
- implicit approach: the process is subdivided into successive steps where the force equilibrium is verified.

As metal forming processes often mean large material flow, the choice of a Lagrangian approach has to be associated with a remeshing procedure as some finite elements become strongly distorted during the simulations. An automatic two-dimensional remeshing module [9,10] has been developed:

- automatic remeshing decision based either on geometric element criteria or on error estimators,
- generation of a new mesh according to the updated contour line and to a variable mesh density that induces mesh refinement or mesh coarsening adapted to error analysis or geometric element criteria,
- transfer of velocity field, internal variables and stress tensor between the old mesh and the new one,
- restart of the simulation.

In swaged bolts, the collar forging could require remeshing procedure. However the geometric quality of the deformed elements without remeshing has shown that this step is not required for these simulations.

In the field of steel design, *Lagamine* code has already been used for the modelling of beam-to-column connections. Bursi and Jaspart [11,12] propose an overview of the current developments for estimating the moment-rotation behaviour of bolted moment resisting connections. The calibration of the commercial code ABAQUS on test data of elementary tee stub connections as well as simulations by Lagamine code were initially performed to scrutinise issues related to discretization, element type, constitutive laws and step size. Next an assemblage of three-dimensional beam finite elements was proposed to model the bolt behaviour in a simplified

yet accurate fashion.

To study the behaviour of swaged bolts in loaded structures is a future goal, this paper focuses on its installation process to provide a better understanding of the phenomena happening during this step. It must not be forgotten that the initial stress distribution in the bolt as well as its geometry, result from this installation process.

3.2. Solid element

The bolt geometry allows an axisymmetrical state to be assumed and two dimensional elements to be used. The temperature increase due to friction and plastic dissipation is limited and a thermo-mechanical analysis is not required, so mechanical simulations were performed. In practice, the Lagamine code proposes three types of two-dimensional mechanical solid elements:

- PLXLS [4]: classical isoparametric element based on the virtual work principle expressed according to the displacement field, the numbers of nodes and integration points are variable but in general, parabolic case with sub integration is adopted (8 nodes and 4 integration points);
- JET2D [13] and BLZ2D [14] are mixed type elements with four nodes and one integration point. They are based on the Hu-Washizu principle which is formulated on three fields: displacement, strain and stress. Special cares such as anti-hourglass stresses and assumed strain method are taken to avoid spurious zero-energy modes and incompressibility locking. Different assumptions on these topics have resulted in two distinct elements.

The helical grooves present in the pin at the initial state and also in the collar at the final state justify PLXLS choice with eight nodes and four integration points. In fact, this parabolic element brings an accurate geometric description with a limited number of degrees of freedom.

The installation of a swaged bolt takes into account five bodies: the pin, the collar, two plates and the hydraulic tool. The model discretizes only three bodies by solid elements: the pin, the collar, and a "work piece" representing the two plates as the friction and discontinuity between these plates do not affect the installation process if perfect flat plates are assumed. The hydraulic tool is simulated by a rigid moving body, defined by a boundary contact condition. For each discretized body, the contour line is given to an automatic mesh generator which provides the solid elements mesh.

3.3. Contact element principle

The contact is the main feature of the swaged bolt simulation as the loading of each body comes from the contact and friction conditions. It is simulated by an interface element based on a penalty approach and derived from the virtual work principle [15]. Kinetically compatible with the associated solid element, this element is defined by an isoparametrical approach and its numerical integration is carried out by Gaussian points. For some special choice of reduced integration scheme, this element is equivalent with a mixed one, based on a multi-field variational principle [16]. The originality of the present approach lies in the fact that the contact conditions (Signorini's condition and Coulomb friction law) are expressed at some integration points, not at the nodal points.

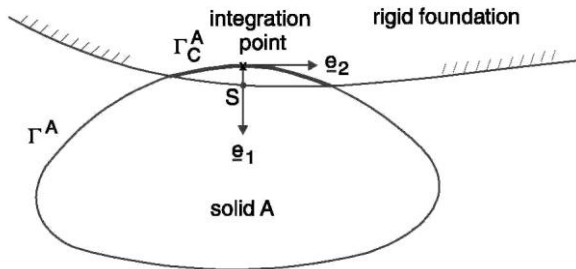
The development of contact between deformable solids A and B introduces a coupling between the degrees of freedom (DOF) of each body. A simple way to treat this kind of problem is to neglect this coupling. This case called "uncoupled approach" means that at a given time t , the geometry of solid A is "frozen" and the contact elements belonging to solid B "see" the boundary of solid A as a rigid foundation. Reciprocally, at the same time t , the contact elements belonging to solid A are also calculated as if the geometry of solid B was frozen. Hence, the contact forces computed by the contact elements of each solid depend only on the DOF of this solid. As the stiffness matrix used to iterate and to find the force equilibrium is computed by the force derivatives, in this uncoupled approach, the stiffness matrix has no term that couples DOF of solids A and B .

On the contrary, if the contact forces are computed exactly and depend on the DOF of the two solids, then the corresponding stiffness matrix establishes a full coupling between the DOF belonging to the boundary of each solid. This approach is called the "coupled approach". The uncoupled approach [15] yields no convergence if solids A and B have similar stiffness. The present swaged bolt simulation is an additional example.

3.4. Contact law

The contact law formulation is related to an elastic-plastic formalism with an elastic field (sticking contact) and a plastic field (sliding contact). In this context, the yield surface is expressed by the dry Coulomb friction formula. For simplicity, this law is presented here for the uncoupled case but Ref. [15] gives all the details for coupled case. Fig. 3 defines the solid A, its total boundary: Γ^A , its contact boundary: Γ_c^A and the rigid foundation that enters into contact with solid A.

Fig. 3. Definition of contact geometry and local axes.



Contact happens when a penetration between the foundation and the solid is detected. This small interpenetration of the solids results from the used penalty concept. Local axes are defined at each integration point (Fig. 3) of the contact boundary Γ_c^A with e_1 inside normal and e_2 tangent to Γ_c^A , note that this boundary is assumed to be smoothed. The contact stresses: the pressure p and the tangential stress τ are oriented according to the local axes e_1, e_2 . In fact, this non-linear approach works with the contact stress rates: $\dot{p}, \dot{\tau}$. The strain rates \dot{e}_1, \dot{e}_2 are the relative velocity components expressed in local axes of the integration point belonging to solid A and the boundary point S of the foundation (Fig. 3). The case of sticking contact corresponds to the elastic case in the present analogy with elastoplastic formalism. The stress and strain rates are linked by the relationship (1) in sticking case:

$$\begin{pmatrix} \dot{p} \\ \dot{\tau} \end{pmatrix} = \begin{pmatrix} K_p & 0 \\ 0 & K_\tau \end{pmatrix} \begin{pmatrix} \dot{e}_1 \\ \dot{e}_2 \end{pmatrix} \iff \dot{\sigma} = \underline{C} \dot{\epsilon} \quad (1)$$

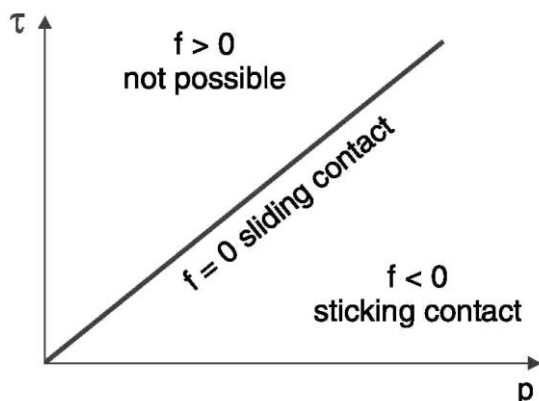
where K_p, K_τ are the penalty coefficients. They are chosen as large as possible to reduce solid interpenetration and still to give convergence of the Newton-Raphson iterative procedure that computes force balance. The friction or sliding contact case represents the plastic case. Its appearance depends on a yield locus expressed by Coulomb condition (Fig. 4):

$$f = |\tau| - \phi p = 0 \quad (2)$$

where Φ is the friction factor. In metal plasticity (standard or associated plasticity), the normality law is used to express the plastic strain rate:

$$\dot{\epsilon}^p = \lambda \left(\frac{\partial f}{\partial \sigma} \right) \quad (3)$$

Fig. 4. Sliding Coulomb criterion in stress space.



where λ is the plastic factor. In contact model, this law cannot be applied because no plastic strain is associated to the contact pressure. This justifies why, a non-associated plasticity law is chosen, where the function f is replaced by function g :

$$g = |\tau| \Rightarrow \dot{\epsilon}^p = \dot{\lambda} \left(\frac{\partial g}{\partial \sigma} \right) \quad (4)$$

The relation between stress and strain rates in friction case can be written as:

$$\begin{pmatrix} \dot{p} \\ \dot{\tau} \end{pmatrix} = \left(\begin{pmatrix} K_p & 0 \\ 0 & K_\tau \end{pmatrix} - \begin{pmatrix} 0 & 0 \\ -\phi K_p \frac{\tau}{|\tau|} & K_\tau \end{pmatrix} \right) \begin{pmatrix} \dot{\epsilon}_1 \\ \dot{\epsilon}_2 \end{pmatrix} \quad (5)$$

4. Swaged bolt modelling

4.1. Mechanical characteristics of swaged bolts

During the installation, permanent deformations are observed in the collar. They are due to the forging process of the collar between the pin and the anvil. Several mechanical phenomena can be remarked: the elastic-plastic behaviour of the pin and collar steels, the friction contact between the anvil and the collar, the progressive damage of the breaking groove and the dynamic effect resulting by the break of this breaking groove. As poor knowledge on the materials is available, it is not possible to use a damage law [17], which could model more accurately the pin break. A classical isotropic elastic-plastic law of Von Mises type with simple bilinear stress-strain curve is adopted for all the present materials. The considered mechanical characteristics of the whole model are given in Table 1.

Table 1 Mechanical characteristics of each component

	Young's modulus (MPa)	Yield stress (MPa)	Strain hardening modulus (MPa)
Pin	210,200	1170	2500
Collar	204,200	313	2090
Plates	210,000	235	0

(a) *Mechanical characteristics of the pin.* The dimensions of the pin are sufficient to allow standard tension test coupons to be extracted. Some tests have been performed by Czarnomska et al. [1], some other ones have been obtained more recently [18]. They can be represented by a bilinear law which is used at the simulation level as natural strain-true stress reference curve (Fig. 5(a)).

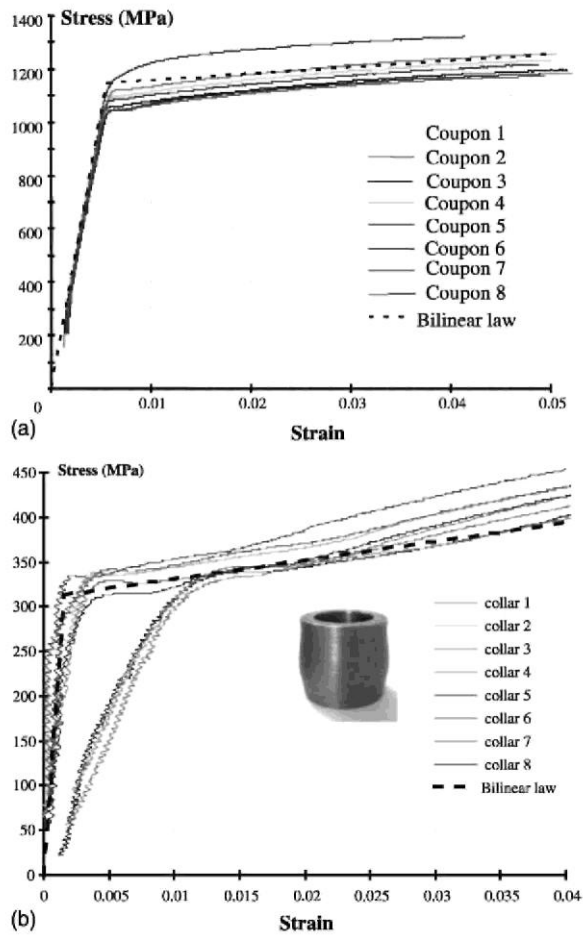
(b) *Mechanical characteristics of the collar.* Because of the small sizes of the collar, it is not possible to machine classical tensile test coupons. So, it was decided to carry out compressive tests on small ring-samples cut in collars. This testing series present two aspects. The first aspect is the crushing test of the cylindrical sample measuring the displacement of the moving table. The second aspect is a test (*Blank* test) without any sample in order to measure the compressive flexibility of the testing machine. The displacement values of both tests are subtracted for the same value of crushing force. These last results (Fig. 5(b)) are the most reliable results according to classical steel values.

(c) *Mechanical characteristics of the steel plates.* The steel plates are made of S235 steel grade. No specific tests were performed, elastic modulus and yield stress come from literature. No strain hardening is taken into account.

(d) *Friction coefficient.* A correct modelling of the installation must take into account the forces transmitted by the friction between the anvil and the collar. To define the relevant friction coefficient between the collar and the anvil, the barrelling of the ring-samples during compression tests of the collar was measured. The covering of the sample support surfaces was adapted to be as close as possible to the real friction conditions. Then, finite element simulations of this test have been conducted with the stress-strain curve defined on point (b) associated to various friction coefficients. Comparing the force and the final shape between experiment and numerical

models, it has been possible to get the best value for this coefficient: 0.05. For the other contacts (plates/pin, plates/collar and pin/collar) no information was available and 0.15 value is adopted as it is known as being reasonable in deep drawing when no special care is applied.

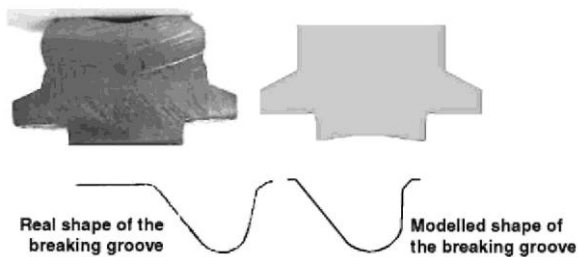
Fig. 5. (a) Strain-stress curves of the pin and (b) strain-stress curves of the collar.



4.2. Geometrical characteristics of swaged bolts

The bolt shape leads to the chosen axisymmetrical model. The hexagonal flange of the collar and the head of the pin are approximated to cylinders with the same normal sections (Fig. 6).

Fig. 6. Actual and modelled shapes of the pin-head and of the breaking groove.



(a) *The pin:* The profile of the head is kept but a cylinder with the same cross-sectional area replaces the hexagonal part. The equivalent diameter ϕ_{eq} is calculated using a formula where ϕ_{ins} is the diameter of the inscribed circle and ϕ_{cir} , the drawn round circle diameter:

$$\phi_{eq} = \sqrt{\left(\frac{3\phi_{ins}\phi_{cir}}{\pi}\right)} \quad (6)$$

The helical grooves of the pin are transformed into fluting but keeping the actual non-symmetrical profile. All the dimensions are chosen as close as possible to the theoretical or nominal manufacturer data and to data obtained by profile projections (Fig. 7). The pintail keeps its real length, 54 mm. And, to respect the full mechanical behaviour during the installation, the breaking groove is also represented as accurately as possible (Fig. 6). The dimensions of its profile are also obtained by profile projection measuring.

(b) *The collar:* As the pin, it is more or less cylindrical. As previously, the hexagonal flange is replaced by a cylinder with the same cross-sectional area in order to keep the same contact area (Fig. 8). The dimensions are also taken from a profile projection measuring.

(c) *The plates:* One cylinder only models the plates. The value of its external diameter is chosen large enough to allow a realistic stress diffusion to be provided. The manufacturer gives the value of the internal diameter.

Fig. 7. Thread dimensions.

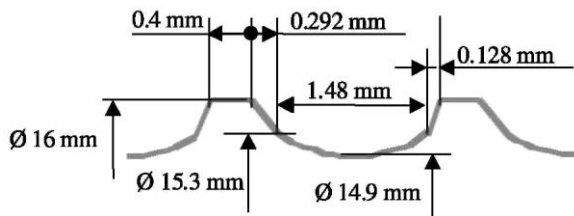
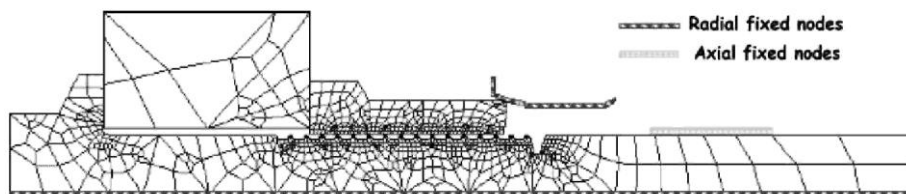


Fig. 8. Collar 16 mm diameter: actual and modelled shapes.



Fig. 9. The whole model of the parametrical study.



4.3. Global mesh

Fig. 9 shows the whole FEM model including the pin, the collar, the steel plates (represented by one rectangle) and the anvil.

4.4. Installation load evolution

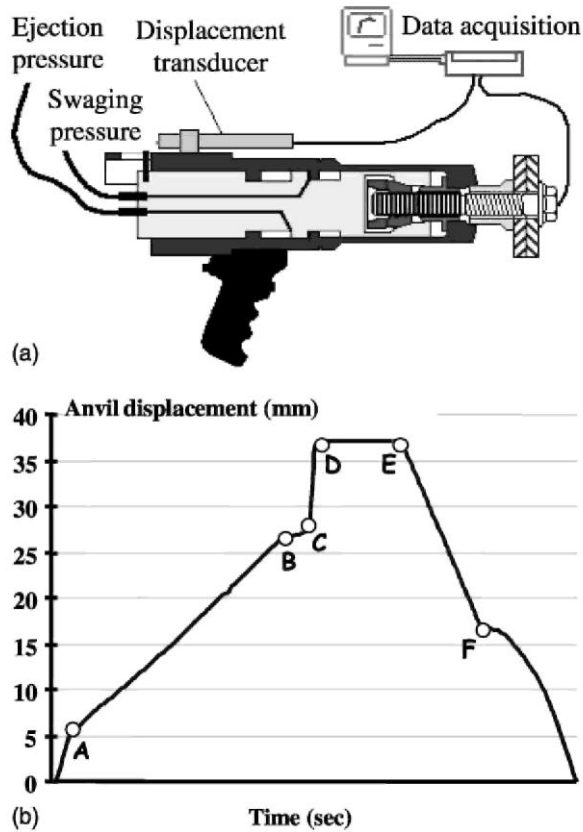
In order to calibrate the parameters governing the mechanical behaviour of the installation process, it was necessary to define some reference steps. As it is not possible to measure the forces developed by the hydraulic tool during the installation, the first reference step is chosen to be the displacement of the anvil measured by a transducer fixed on the body of the installation tool (Fig. 10(a)). A typical curve representing the evolution of this displacement versus the installation time is shown on Fig. 10(b). Point A marks the creation of the first thread in the collar. The swaging process ends at point B and the anvil action stops at point C. The break of the breaking groove occurs at point D and the anvil begins to come back at point E.

The loading evolution is calibrated to follow the evolution of the forces applied to the body of the installation tool. The hydraulic power unit imposing the pressure on the piston, creates the force on the anvil. The calculation is carried out in two steps. The first one is the swaging of the collar onto the pin (Fig. 10(b), between A and B), the second one is the withdrawal of the tool from the collar (Fig. 10(b), after E to the end of the curve). Computations are governed by displacements.

4.5. Representation of the contacts

Concerning the contacts, different techniques were tested. The conclusion of these tests is that the best modelling method, if not the only possible one, is the coupled approach for collar/pin and collar/plates contact, mainly because the stiffness of all these solids is very close. The uncoupled approach is only used for the collar/anvil contact, which is classical as the anvil is not meshed but simulated by a moving boundary with infinite stiffness (foundation).

Fig. 10. (a) Measure of the hydraulic tool displacement and (b) measured displacement of the hydraulic tool.



4.6. Computations

The computations were carried out in two sequences. The first one was achieved to check the validity of the model, the second one to analyse some parametrical influences. During the second sequence, and to allow modifying the numerical conditions of the computation, the whole-modelled swaging process is divided into different steps. Indeed, the beginning of the calculation reveals to be critical, due to the required penetration to initiate contact between the anvil and the collar. The preexisting force generates a numerical bound due to the contact strategy. Lowering the non-equilibrated forces attenuates this effect but slows down the computation. Then, in the following, this effect is reduced. The choice of the loading step is automatically adapted within the performance of the convergence. Only the minor value and the major value of the step size are determined by the user.

5. Results

5.1. First computations

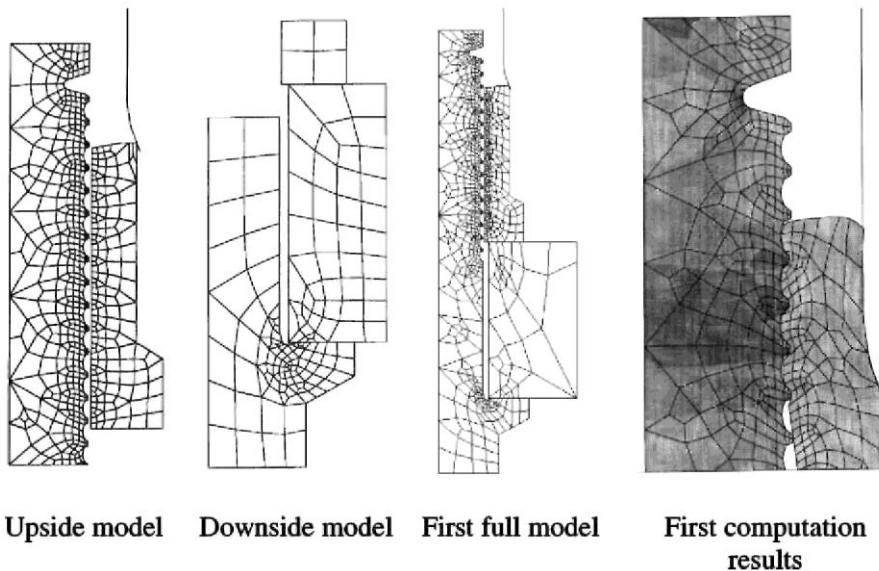
During the first sequence of calculations, the model was divided into two parts, the upside part with the collar and the downside part with the head pin and the plates (Fig. 11).

Both computations were carried out to check that the contact phenomena do not induce any problems of convergence. The results showed that each part could be calculated during the swaging process but also during the anvil withdrawal.

The deformations of the meshes are almost the same as the actual bolt, however high penetration between solids appeared. Using higher penalty coefficients reduces this penetration between the meshes for next models.

The pintail size appears to be too influential so it was decided to keep its real length and its real shape in the final model. Indeed, the stress flow is better respected with a long pintail and with fixed nodes further located on the pintail (Fig. 9).

Fig. 11. First tests of computation meshes.



5.2. Swaged geometry of the parametrical study

The whole bolted joint is modelled now. Both parts previously described are gathered and comparisons are made on the collar geometry.

Firstly, the shape of the collar mesh at the end of the numerical installation is compared with the shape of a real swaged collar cut in the middle (Fig. 12). The mesh matches very well with the filling up of the real pin threads:

- the threads at the top of the collar present gap with the pin, because of the hold of the anvil on the collar flange at the end of the swaging process,
- the threads in the middle of the collar are well formed,
- the threads at the bottom of the collar are nearly absent. In fact, the threads begin at the top of the collar flange.

Fig. 12. Cut sample of swaged bolt and mesh at the end of the numerical installation.

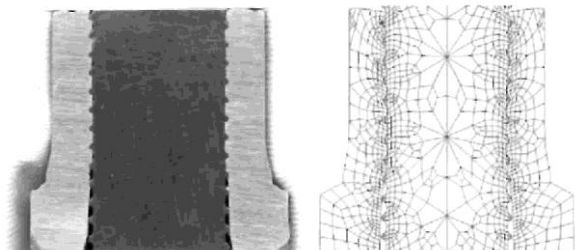


Table 2. Geometrical dimensions taken on the swaged collar

Data type	Swaged diameter at the collar top (mm)	Swaged length (mm)
Test average	23.97 ($\sigma = 0.012$)	19,9 ($\sigma = 0.23$)
Modelling results	23.98	20.35
Control data	24.1 max	17.7 min

An actual swaged bolt installation can be controlled by some specific dimensional data provided by the manufacturer (control data), such as the length of the swaged part of the collar. Therefore, it was decided to control the numerical installation with this criterion.

The diameter values of the modelled swaged collar vary from 23.98 mm at the top, to 24.14 mm at the bottom. The experimental values can only be measured at the top because of the accessibility of the measurement tool (calliper rule). The swaged length is measured with a ruler and according to the manufacturer method. All the experimental values match with the controlled values and verify well the numerical modelling values (Table 2).

5.3. Forces acting during the installation

(a) *Internal load.* Installation tests have been used to compare the numerical results to the actual behaviour. They consist in measuring the internal load in the pin in function of the displacement of the anvil during the installation. The internal load is measured with an axial gauge glued in the shank zone of the pin [2]. So, it is possible to obtain a preload-displacement curve (Fig. 13).

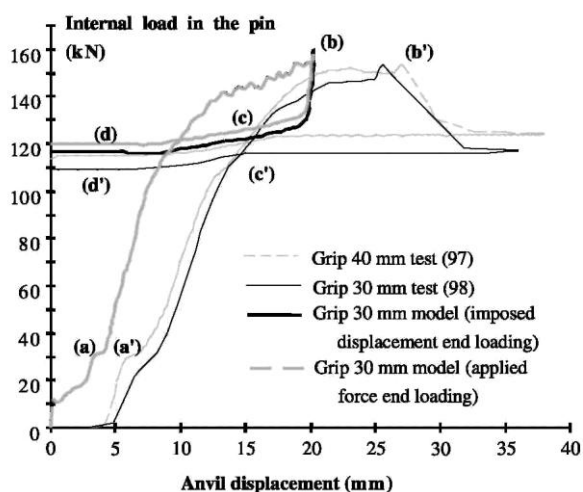
In the computation, the tension in the pin is deduced from the stress value obtained in the finite element corresponding to the gauge location. The displacement is chosen to be equal to the tool displacement. Therefore, another internal load-displacement curve can be plotted (Fig. 13).

Curves shown in Fig. 13 have the same shape. Point(a) and point (a') mark the creation of the first thread in the collar and the collar blocking on the pin. The internal load value reaches 31 kN in the numerical installation and in the experimental installation. Point (b) and point (b') mark the end of the swaging process. It corresponds to the point where the final external load value is the highest.

Small differences appear about the final preload. The loss of preload observed on the numerical curves can be explained by the strategy of computation. Imposing the displacement allows the material to flow; this creates a force decreasing. The differences of loading levels at each step of the installation are due to the variations of the mechanical characteristics and of the dimensions of the tool. Notably, the level of preload at the end of the loading is mainly sensitive to the value of the strain hardening modulus of the pin. Regarding the preload at the

end of the tool ejection, it appears to be lower than the actual value. The dimensions, but also the shape of the tool, affect this preload.

Fig. 13. Numerical and experimental internal load-displacement curves.



According to these numerical and experimental results, a comparison of the tensile forces in the pin is made for each key-step of the installation (Table 3). The only anvil withdrawal phase is not mentioned because it corresponds to a variation of the tensile force. The comparison of these different values shows that the dimension order between the experimental data and the numerical data is kept.

(b) *Internal contact forces during the installation.* To check each solid equilibrium, the contact forces between each of them are calculated and represented (Fig. 14).

During the swaging process, the axial contact force between the plates and the pin is the addition of:

- the contact force between the pin and the collar,
- the external load.

Three forces are applied on the pin:

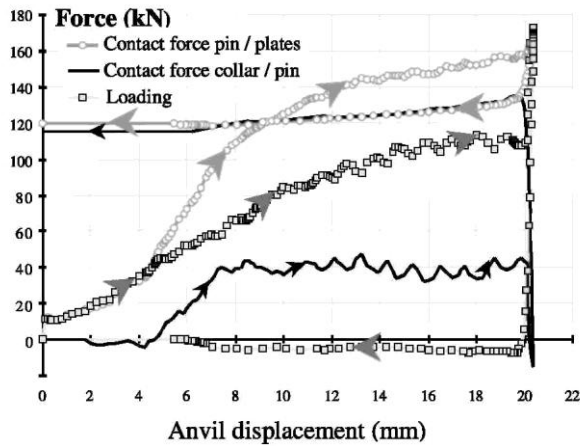
- the internal load in the pin itself,
- the tool action,
- the reaction due to the collar expansion,

this system being mechanically equilibrated during the swaging process.

Table 3. Forces in the pin at the key moments of the installation

Source	Higher force in the pin (b) (kN)	Final preload (d) (kN)	Loss of force at the breaking groove break (kN)
40 mm grip test	154.6	114.8	39.8
30 mm grip test	148.9	105.6	43.3
30 mm grip model (displacement stop)	159.6	117	42.6
30 mm grip model (force stop)	157.8	120.25	37.55
Manufacturer documents	-	>113.4	-

Fig. 14. Computed forces between the different components of the bolt.



Then, during the anvil withdrawal, the loading force applied by the anvil becomes negligible. So, the contact force between the collar and the pin has the same values as the contact forces between the other solids (plates/collar and plates/pin). Two equal forces equilibrate each solid. This statement confirms the correct mechanical equilibrium of the model.

Fig. 15 represents the ways taken by the actions between the solids during the installation process. Before the creation of the first thread in the collar and so, before the creation of the contact force between the collar and the pin, two forces equilibrate all the solids. This is why, the axial projections of these forces are equal, notably the external load and the force in the pin. During the swaging process, a new action appears between the pin and the collar. At the beginning of this process, it reacts against the external load. But, when the threads in the collar are strong enough, the contact force between the collar and the pin changes and increases the applied load. This sign change is due to the axial expansion of the collar limited by the plates and the threads.

When the breaking groove breaks, the loading action moves to the contact between the collar and the pin. And again, two forces mechanically equilibrate the solids.

The anvil withdrawal shows a small force due to the friction between the anvil and the collar. The last equilibrium is not modified by this force which is too small. The loss of force in the pin comes from the released circular stress.

Fig. 15. Loads acting during the installation sequences.

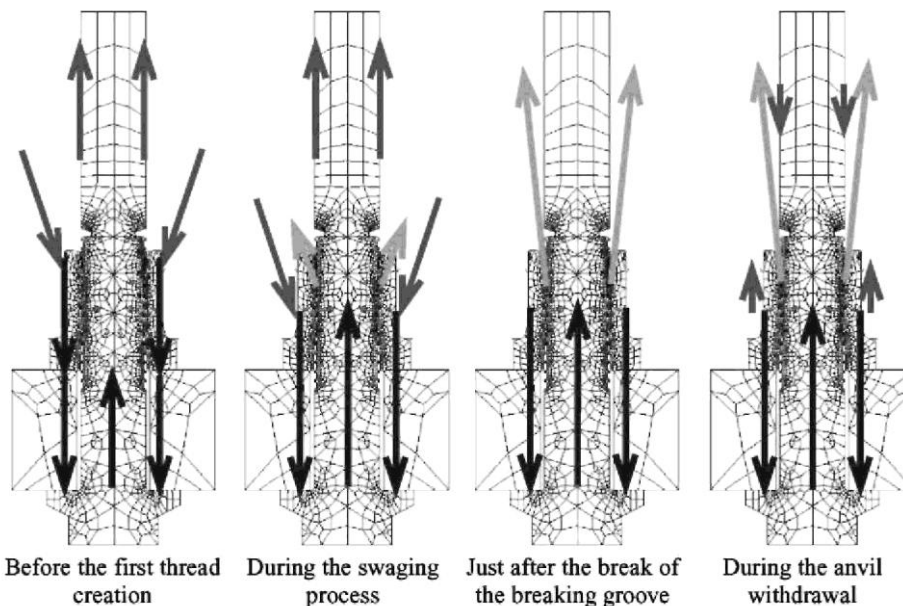
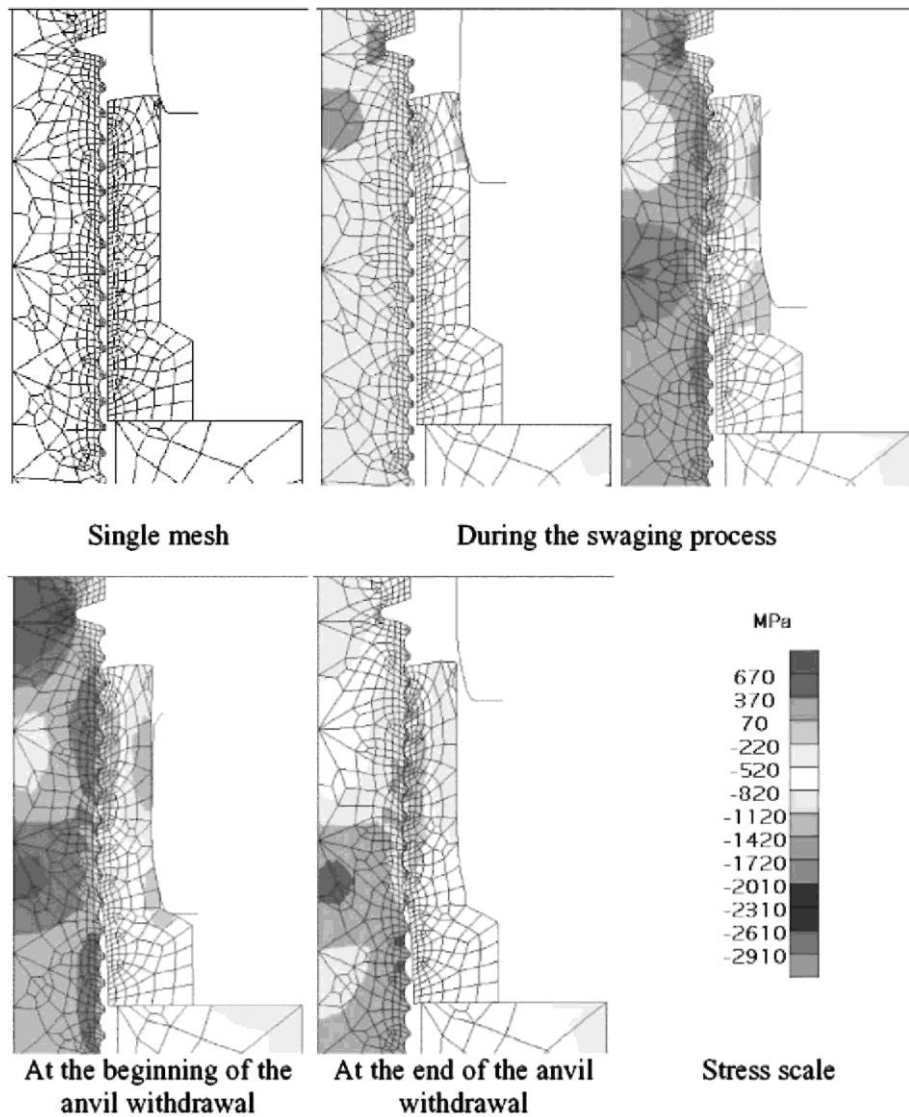


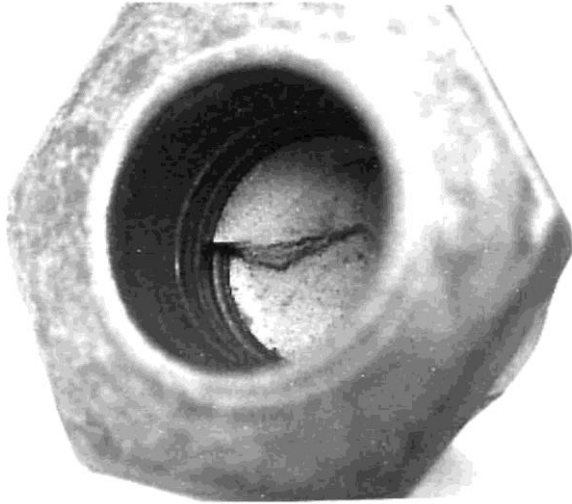
Fig. 16. Axial stresses.



5.4. Stresses in the bolt during the installation

A zone of high stress values can be noticed in the pin, which follows the displacement of the anvil during the swaging process (Fig. 16). At the beginning of the anvil withdrawal, the axial stress value reaches 500 MPa in this area, nearly equal to the stress in the breaking groove zone (570 MPa). Then, this zone of high stress values remains at the same place but the value of the axial stress decreases down to 400 MPa. It represents 44% of the yield stress of the pin material. This particular zone corresponds to the location where, in the pin, a fatigue fracture appears under low-cyclic loading [2] (Fig. 17).

Fig. 17. Broken pin in the collar after low-cycle fatigue test.



6. Conclusions

Modelling of the installation process of swaged bolts represents several mechanical steps, which cannot be approached by tests. This is due to the fact that the small size of the collar does not allow any fine instrumentation to be installed. So, a numerical model is required which needs to use a simulation technique able to represent the large strains associated with the collar forming process on the pin.

In a first phase, a detailed modelling of a swaged bolt has been presented considering both the pin and the collar. Then, the software Lagamine, based on the FEM and especially written for large distortions and large displacements, has been chosen to compute all the different mechanisms involved during the different swaging steps.

The pin, the collar and the steel plates are modelled as close as possible to their actual shape and to their accurate mechanical characteristics, these last ones being deduced from several tension or compression tests refined with a numerical analysis.

To represent the real shape of the anvil, the modelling of the tool is carried out using rigid lines. Its displacements govern the computation. The Coulomb friction law is used to model the contact between the different meshes. The numerical results are compared to the experimental ones, which are carried out by measuring the force with a strain gauge located in the shank zone of the pin. The differences, which appear in the general behaviour, are due to the difference between the mechanical characteristics taken for the computation and the actual ones. The simulations allow the sensitivity of some parameters to be evaluated (the strain hardening of the pin or the tool shape for instance).

This numerical approach gives efficient information about the behaviour of a swaged bolt at each step of the installation process. It allows the detailed stress distribution to be established with reasonable accuracy. This leads to better understanding of the parameters acting a role in the mechanical behaviour of this new fastener, and clarifies the sensitivity of the collar swaging process.

This study shows that the characteristics of each component (pin or collar) have a strong influence on the mechanical behaviour during the installation, but also that the diameter, and more surprisingly the shape of the tool, is also very influential on the history of the preload value.

References

- [1] Czarnomska M, Muzeau JP, Racher P. Étude expérimentale comparative du comportement d'assemblages par boulons sertis Huck-Fit ou par boulons HR 10.9. *Construction Métallique* 1993; 2:9-29.

- [2] Missoum A. Étude expérimentale de boulons sertis précontraints utilisés en construction métallique. PhD thesis, Blaise Pascal University, Clermont-Ferrand, France, 1997.
- [3] Baptista AM, Missoum A, Muzeau JP, Ryan I. Testing of swaged bolts for steel connections. In: International Conference New Technologies in Structural Engineering, NEW TECH'97, Lisbon, Portugal. 1997. p. 589-94.
- [4] Cescotto S, Grober H, Perdrix C. Calibration of an elastic-visco-plastic constitutive equation for steels in the hot-rolling conditions. In: Middleton J, Pande GN, editors. Numerical methods in engineering: theory and applications, Balkema, vol 1. Balkema; 1985. p. 393-9.
- [5] Li K, Habraken AM, Bruneel H. Simulation of square cup deep drawing with different finite elements. J Mater Process Technol 1995;50 (1-4):81-91.
- [6] Charles JF, Castagne S, Zhang L, Habraken AM, Cescotto S. Numerical modelling of the forging process of rolls for rolling mills. In: Pietrzyk M, Kusiak J, Majta J, Hartley P, Pillinger I, editors. Metal forming 2000. Balkema; 2000.
- [7] Habraken AM, Charles JF, Wegria J, Cescotto S. Dynamic recrystallization during zinc rolling. Int J Forming Processes 1998; 1.
- [8] Duchêne L, Habraken AM, Godinas A. Implementation of a texture based interpolated yield locus in FEM code. In: Mori, editor. NUMIFORM simulation of materials processing: theory, methods and applications, 18-20 June 2001. Tokyo: Balkema Publishers; 2001.
- [9] Habraken A-M, Cescotto S. An automatic remeshing technique for finite element simulation of forming processes. Int J Numer Meth Eng 1990; 30:8.
- [10] Dyduch M, Habraken A-M, Cescotto S. Automatic adaptive remeshing for numerical simulations of metal-forming. Comput Meth Appl Mech Eng 1992; 101.
- [11] Bursi OS, Jaspert JP. Finite element-based models for the analysis of bolted beam-to-column steel connections. Colloquium Istanbul 96 semi-rigid structural connections. HÖnggerberg Zürich: IABSE-AIPC-IVBH ETH; 1996.
- [12] Bursi OS, Jaspert JP. Basic issues in the finite element simulation of extended end plate connection. J Struct Eng 1998;69: 361-82.
- [13] Jetteur P, Cescotto S. A mixed finite element for the analysis of large inelastic strains. Int J Numer Meth Eng 1991;31: 229-39.
- [14] Zhu YY, Cescotto S. Transient thermal and thermomechanical analysis by FEM. Comput Struct 1994; 53 (2):275-304.
- [15] Habraken AM, Cescotto S. Contact between deformable solids, the fully coupled approach. Math Comput Modell 1998;28 (4-8):153-69.
- [16] Habraken AM, Bourdouxhe M. Coupled thermo-mechanical-metallurgical analysis during the cooling of steel pieces. Eur J Mech: Solids 1992; 11 (3):381-402.
- [17] Cescotto S, Charlier R. Frictional contact finite element based on mixed variational principles. Int J Numer Meth Eng 1993; 36: 1681-701.
- [18] Dréan M. Étude expérimentale et numérique de la mise en oeuvre de boulons sertis. PhD thesis, Blaise Pascal University, Clermont-Ferrand, France, 1999.